A Linear Control Approach to Design Digital Speed Control System for PMSMs

Xin Yuan, *Member, IEEE*, Jiahao Chen, *Member, IEEE*, Wei Liu, *Member, IEEE*, and Christopher H. T. Lee, *Senior Member, IEEE*

***Abstract*—In order to pursue the high performance of speed control for permanent magnet synchronous machines (PMSMs), a digital speed control system is proposed. In the proposed structure, two parts, namely, speed controller and speed measurement, have been designed compared with the conventional speed control scheme. The proposed universal instantaneous speed observer is regarded as the speed measurement, where it can unify other types of speed observer, eliminate delay issue, and reduce measurement noises by utilizing the merit of high-order system characteristic. The proposed speed controller with an active damping structure is able to decouple the current loop bandwidth effect on the speed system; meanwhile, it possesses better dynamic response, disturbance rejection, parameter robustness, and measurement noise suppression compared with other types of speed controller. In addition, the proposed digital speed control system in the z domain is analyzed in detail. The theoretical effectiveness of the proposed design is verified in a PMSM test rig.**

***Index Terms*—Digital speed control, permanent magnet synchronous machines (PMSMs), speed observer.**

NOMENCLATURE

$\mathbf{U}_{dq}, \mathbf{e}_{dq}$	Stator voltage and back EMF voltage.
$\mathbf{i}_{dq}, \mathbf{i}_{dq}^{\text{ref}}$	Measured and reference stator current.
$\hat{\omega}_m, \omega_m^{\text{ref}}$	Evaluated and reference mechanical angular speed.
T_s	System sampling and control period.
L_d, L_q	dq-axis stator inductance.
R_s, p	Stator resistance and pole pair number.
$J, \overline{J}$	Actual and nominal inertia.
$K_t, \overline{K_t}$	Actual and nominal torque constant.
T_e, T_e^{ref}	Actual and reference electromagnetic torque.
$\hat{T}_l, T_l$	Evaluated and actual load torque.
$\hat{\theta}_m, \theta_m$	Evaluated and actual mechanical angle.
$\omega_c, \omega_{\text{ob}}$	Current loop and speed observer angular frequency.
ω_{spd}	Speed controller angular frequency.

Manuscript received October 25, 2021; revised December 7, 2021; accepted January 21, 2022. Date of publication January 27, 2022; date of current version March 24, 2022. This work was supported by the National Research Foundation (NRF) Singapore, under the NRF Fellowship under Grant NRF-NRFF12-2020-0003. Recommended for publication by Associate Editor L. V. Iyer. *(Corresponding author: Christopher H. T. Lee.)*

Xin Yuan, Jiahao Chen, and Christopher H. T. Lee are with the School of Electrical and Electronic Engineering, Nanyang Technological University, Singapore 639798 (e-mail: yuanxinedu@gmail.com; jiahao.chen@ntu.edu.sg; chtlee@ntu.edu.sg).

Wei Liu is with the Department of Electrical and Electronic Engineering, The University of Hong Kong, Hong Kong (e-mail: liuwei@eee.hku.hk).

Color versions of one or more figures in this article are available at https://doi.org/10.1109/TPEL.2022.3146174.

Digital Object Identifier 10.1109/TPEL.2022.3146174

I. INTRODUCTION

A. Literature Review

PERMANENT magnet synchronous machines (PMSMs) are becoming a trend for ac servo applications, and the speed control of PMSMs is expected to exhibit more high performance [1]. The speed control is generally nonlinear and time varying due to model parameter uncertainty and external disturbances, including cogging torque, friction torque, and unknown load torque. Current loop (inner loop) [2], speed measurement, and speed controller commonly constitute the overall speed control system [3].

It is well known that the speed measurement should be obtained by position sensors, i.e., resolver sensor, Hall effect sensor, and magnetic encoder sensor. Although sensorless technology can replace position sensors, it cannot totally guarantee the desired performance within the wide speed and torque range and inaccurate motor parameters [4]. Based on position sensors, there are four typical measurement approaches, i.e., digital filter, phase-locked loop (PLL), Kalman filter [5], and instantaneous model-based speed observer. The digital filter can effectively eliminate the measurement quantization noises [6] but induce phase lag, which can dramatically deteriorate the overall speed control system performance. The PLL requests the involvement of hardware and is actually a frequency filter [7]. The Kalman filter is relatively complex and usually takes the quantization error as Gaussian noises. The noise model may be different with real noises. Lorenz and Van Patten [8] proposed an instantaneous model-based speed observer, in which the observer can eliminate the speed delay issue based on the actual system model. Based on the observer structure, a cascade speed observer is proposed to reduce the quantization noises, but the calculation is relatively complicated due to the involvement of multiple observers [9]. Aiming to improve speed estimation performance at a low-speed region, several improved approaches based on the model-based observer have been proposed [10]–[12]. In the field of low-revolution position sensors, the speed estimation and position estimation should be both carried out, and they cannot be achieved in only one observer scheme. In order to solve this issue, two observers are developed to enhance speed and position performance at the same time: one is for the speed estimation and the other is for the rotor angle position estimation [4], [13].

An ideal speed controller should have the best speed reference tracking, external disturbance rejection, measurement noise suppression, and strong parameter robustness. With the

development of speed controllers, proportional–integral (PI) type and P-type speed controllers have been widely utilized in modern industrial applications. The conventional PI-type speed controller inherently owns the disturbance rejection, but there exists a slight speed overshoot phenomenon since a zero exists in the speed closed-loop transfer function [14]. In order to improve the above issue, scholars have developed two-degree-of-freedom (DOF) speed controllers [15]. Harnefors *et al.* [16] proposed a classical two-DOF PI speed controller by adding an active damping term, and this structure can avoid the speed overshoot without affecting the dynamic speed tracking performance. In addition, they proposed a novel second-order two-DOF PI-type speed controller by adding a feedforward term, which can effectively eliminate the steady-state error for trapezoidal speed reference [17]. However, the speed measurement part is not considered in the above two-DOF speed controllers. The two-DOF PI-type speed controller can also be employed in the field of model-predictive control (see, e.g., [18]). Considering the speed measurement part, Xia *et al.* [19] developed a speed control system with a two-DOF PI-type speed controller, and the speed dynamic response can be improved further. Employing a high-order nonlinear sliding-mode observer, the speed control system with a two-DOF PI-type speed controller is proposed [20], but the structure is relatively complex due to the involvement of the nonlinear characteristic. Considering the current loop effect on the overall speed control system, the global exponential stability and phase margin of the speed control system have been analyzed [17], [19], [21]. In order to suppress the integral windup in the PI-type controller, a new anti-integral windup PI controller with a separate integral state is proposed [22].

The alternative two-DOF speed controller is the P-type speed controller by employing an instantaneous speed observer [8] or a disturbance observer (DOB). The DOB was proposed by Ohnishi in 1983 and is able to estimate disturbances by using plant model parameters and measured states [23]. The DOB and the instantaneous speed observer can be established by a linear or nonlinear structure and usually taken as a feedforward compensation [24], [25]. The P-type speed controller with a DOB or an instantaneous speed observer is also called active disturbance rejection control (ADRC). In order to reduce the complexity of tuned coefficients, linear ADRC is developed [26]. However, ADRC needs to obtain the speed and disturbances at the same time by utilizing the DOB or the instantaneous speed observer, and the rapid disturbance rejection performance should be traded off with smooth speed estimation performance by using only one observer. Based on this problem, two observers for the speed and disturbance estimation are designed in ADRC, but the system complexity is increased [27], [28].

B. Motivation and Innovation

Considering the speed dynamic response performance, disturbance rejection, measurement noise suppression, current loop model, and parameter robustness, this article proposes a digital speed control system by utilizing a linear control approach. The contributions of this article are as follows.

1) Generally, instantaneous speed observers are based on the angle or speed error to estimate the actual machine speed, and the speed closed-loop transfer function is a fixed third-order system [4], [8], [10]–[13]. In order to establish a universal speed observer, an nth-order internal model control (IMC) instantaneous speed observer based on the superposition theorem is proposed. In this structure, the speed observer is able to unify other types of speed observer, and the design can be easily understood by employing linear control theory. In the proposed speed observer structure, third- and fourth-order observers will be analyzed. With the observer order number increasing, the system stability is deteriorated. In addition, the transfer function from the current and speed quantization noises to the estimated speed is analyzed in detail, which can illustrate that the noises from the position sensor can much more affect the estimated speed.
2) Although two-DOF speed controllers have been proposed, the current loop model is usually neglected. It has been analyzed that when the current bandwidth is high enough, the speed control performance will not be influenced [17], [19], [21], but the speed controller with a relatively low current bandwidth has not been studied in detail. Apart from that, although the ADRC speed controller may be considered as an optimum speed controller because of the simple P-type controller design [26], the speed observer or the DOB needs to estimate the speed and disturbances at the same time. The disturbance rejection performance is coupled with the speed estimation performance, which means that smooth speed estimation and fast disturbance rejection cannot be obtained using a single observer or a DOB. Motivated by the above arguments, a novel speed controller considering a current loop model is proposed, where the undesired coupling effect caused by the current loop model is eliminated. Without introducing the disturbance rejection DOF, an active damping structure is added, and the proposed speed controller can both possess optimum dynamic response and disturbance rejection by adjusting one-DOF ω_{spd}. Utilizing this merit, only one speed observer or DOB is enough for the overall speed control system compared with the ADRC speed control system. Furthermore, in order to enhance the speed loop parameter robustness, a robust coefficient is added in the proposed structure. The robust coefficient can be easily tuned to suppress the effect of $\overline{J}$ and $\overline{K_t}$ parameter mismatch on the overall speed performance. The speed performance evaluation, including dynamic response, disturbance rejection, and measurement noise suppression, has been compared with that in the conventional PI-type and ADRC speed controllers.
3) So far, many literature works only focus on the speed controller or speed measurement (see, e.g., [4], [9], and [17]), but both parts jointly affect the speed performance. Considering this issue, the proposed digital speed control system is established and the performance evaluation will be analyzed. Moreover, since zero-order holder (ZOH) voltage latch and one-step control delay exist in practical

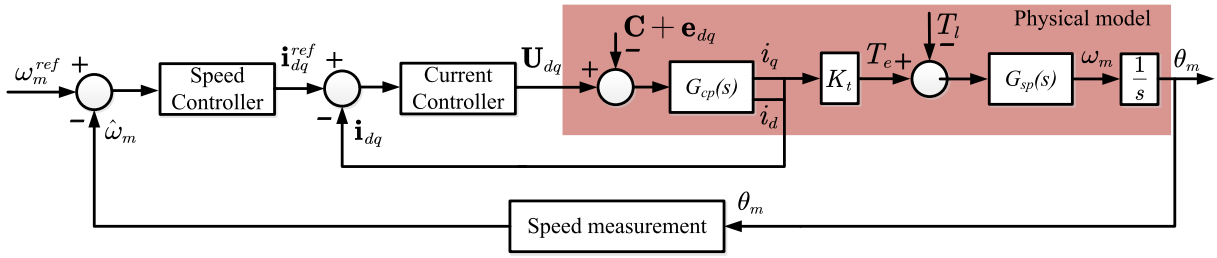

Fig. 1. Block diagram of the speed control system.

systems, the speed control system in the z domain considering two typical current controllers and one-step control delay is established. Based on the discrete-time stability criteria, parameter robustness and the design guidance for tuning α and ω_{spd} are illustrated in detail. In the proposed overall speed control system structure, it can be found that there exists speed performance consistency between the speed controller and the speed observer under parameter uncertainty.

C. Article Organization

The rest of this article is organized as follows. The conventional and proposed speed control systems are introduced in Sections II and III, respectively. Experimental comparison results are presented in Section IV. Finally, Section V concludes this article.

II. Conventional Speed Control System

Generally, a speed control system mainly includes three parts, namely, *current loop*, *speed measurement*, and *speed controller*, as shown in Fig. 1.

In terms of the current loop, inverter nonlinearity and electrical angle delay caused by the ZOH have been fully compensated [29], [30]. Subsequently, the PMSM voltage equations are presented as follows:

$$\mathbf{U}_{dq} = \mathbf{A}\dot{\mathbf{i}}_{dq} + \mathbf{B}\mathbf{i}_{dq} + \mathbf{C} + \mathbf{e}_{dq} \tag{1}$$

where $\mathbf{A}=\begin{bmatrix} L_d & 0 \\ 0 & L_q \end{bmatrix}$, $\mathbf{B}=\begin{bmatrix} R_s & 0 \\ 0 & R_s \end{bmatrix}$, $\mathbf{C}=[-\omega_e L_q i_q, \omega_e L_d i_d]^{\mathsf{T}}$, and $\mathbf{U}_{dq}=[U_d, U_q]^{\mathsf{T}}$. Decoupling of $\mathbf{C}$ and $\mathbf{e}_{dq}$ allows synchronous or asynchronous machines to be modeled by using a resistor–inductor load model. In this article, disturbances caused by PMSM resistance and inductance parameter mismatch have been assumed to be compensated. As a result, using the IMC principle [31], the PMSM model transfer function $G_{cp}(s)$ and the closed-loop transfer function $G_{cl}(s)$ can be presented as

$$G_{cp}(s) = \frac{\mathbf{i}_{dq}(s)}{\mathbf{U}_{dq}(s)} = \frac{1}{s\mathbf{A}+\mathbf{B}}, \quad G_{cl}(s) = \frac{\omega_c}{s+\omega_c}. \tag{2}$$

It should be noted that except for the PI-type current controller, predictive current control can also be employed herein (see [3, Fig. 1]).

Neglecting high-order current harmonics, PMSM motion equations are presented as follows:

$$T_e = K_t i_q, \quad T_l = T_e - J\dot{\omega}_m, \quad \omega_m = \dot{\theta}_m. \tag{3}$$

In order to improve the speed delay issue, an instantaneous speed observer is employed as the speed measurement [8], [27], [28], which can be shown as follows:

$$\begin{cases} \hat{T}_d = K_i \int_0^t (\theta_m - \hat{\theta}_m) d\tau, \quad \hat{T}_l = -\hat{T}_d, \quad \hat{\theta}_m = \int_0^t \hat{\omega}_m d\tau \\ \hat{\omega}_m = \frac{1}{\overline{J}} \int_0^t \left[T_e + \hat{T}_d + K_p(\theta_m - \hat{\theta}_m) \right] d\tau + \frac{K_d(\theta_m - \hat{\theta}_m)}{\overline{J}} \end{cases} \tag{4}$$

where $\hat{T}_d$ denotes the evaluated external disturbances. K_p, K_i, and K_d coefficients of the observer can be selected as $3\omega_{\text{ob}}^2\overline{J}, \omega_{\text{ob}}^3\overline{J}$, and $3\omega_{\text{ob}}\overline{J}$, respectively. The observer can simultaneously evaluate the PMSM speed and external disturbances.

In the field of speed controllers, two classical speed controllers have been developed, namely, PI-type and P-type speed controllers.

1) *PI-type speed controller:* The speed plant and PI speed controller models can be, respectively, described as

$$G_{sp}(s) = \frac{\omega_m(s)}{T_e(s)} = \frac{1}{Js}, \quad G_{sc1}(s) = \frac{K_{p1}s + K_{i1}}{\overline{K_t}s}. \tag{5}$$

The designed coefficients K_{p1} and K_{i1} can be obtained based on a typical second-order system [17], where the values can be determined as $2\omega_{\text{spd}}\overline{J}$ and $\omega_{\text{spd}}^2\overline{J}$, respectively.

2) *P-type speed controller:* However, the speed overshoot phenomenon exists in the PI-type speed controller due to the zero location of the closed-loop transfer function. To avoid this issue, the P-type speed controller is designed. The P-type speed controller with the instantaneous speed observer (4) can predict the load torque T_l and suppress the external disturbances through the feedforward compensation. This structure is also called ADRC speed controller. Without considering $\overline{K_t}$ and $\overline{J}$ parameter mismatch, substituting (3) into (4), the predicted load-torque disturbance $\hat{T}_l(s)$ from the instantaneous speed observer and the P-type speed controller $G_{sc2}(s)$ can be, respectively, expressed as

$$\hat{T}_l(s) = \frac{\omega_{\text{ob}}^3}{(s+\omega_{\text{ob}})^3} T_l(s), \quad G_{sc2}(s) = \frac{K_{p2}}{\overline{K_t}} \tag{6}$$

where the coefficient K_{p2} can be selected as $\omega_{\text{spd}}\overline{J}$.

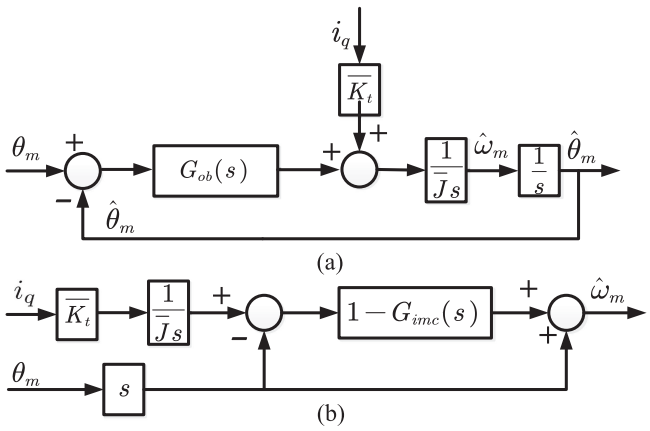

Fig. 2. (a) Speed observer based on the angle error. (b) IMC-speed observer based on the superposition theorem.

III. Proposed Digital Speed Control System

This section presents a proposed digital speed control system based on Fig. 1, where the speed measurement and speed controller parts will be proposed. In addition, the digital speed control system performance evaluation will be presented.

A. Universal Instantaneous IMC Speed Observer

Employing the IMC principle, the proposed IMC speed observer can be applied in the speed measurement. This proposed universal instantaneous speed observer is able to easily unify other types of speed observer. The detailed procedure can be presented as follows.

1) Design Guidance of Universal Instantaneous IMC Speed Observer: First, the input, output, and external disturbance need to be determined. The input and output are the measured mechanical angle of the position sensor and the estimated mechanical speed, while the external disturbance are the actual electromagnetic torque, which is shown in Fig. 2(a). It can be seen that $G_{\text{ob}}(s)$ denotes the designed PI-derivative-based model. Without the external disturbance, it is noticeable that the closed-loop transfer function between the estimated angle and the actual angle can be expressed as $\frac{G_{\text{ob}}(s)\frac{1}{\overline{J}s^2}}{1+G_{\text{ob}}(s)\frac{1}{\overline{J}s^2}}$. Since θ_m is the integral of ω_m, the speed closed-loop transfer function can be obtained once the angle closed-loop transfer function is determined.

Second, without designing $G_{\text{ob}}(s)$, the estimated speed closed-loop transfer function in Fig. 2(a) can be simply solved based on the superposition theorem as shown in Fig. 2(b)

$$\begin{aligned}\hat{\omega}_m &= [1-G_{\text{imc}}(s)]\,\frac{\overline{K_t}i_q}{\overline{J}s} + G_{\text{imc}}(s)\omega_m \\ &= \overbrace{[1-G_{\text{imc}}(s)]\,(\frac{\overline{K_t}i_q}{\overline{J}s} - s\theta_m)}^{\text{Prediction}} + \overbrace{s\theta_m}^{\text{Measurement}}\end{aligned} \tag{7}$$

where $G_{\text{imc}}(s)$ stands for the universal closed-loop transfer function between $\hat{\omega}$ and ω_m. The detailed $G_{\text{imc}}(s)$ design will be presented in the next subsection.

Remark 1: Unlike other speed observers requiring the detailed design of the PI-derivative-based model $G_{\text{ob}}(s)$ and the error between ω_m and $\hat{\omega}$, the proposed universal instantaneous IMC speed observer can only be based on (7) to estimate the speed. Equation (7) is a direct, simple, universal formula to obtain the estimated speed, and it can be seen that the evaluated speed can possess both prediction and measurement characteristic. The prediction part can eliminate the delay issue, while the measurement part can guarantee a high robustness of the IMC speed observer because there is no need to obtain PMSM parameters in the measurement part.

Third, the digital implementation of the IMC speed observer should be established. To make a continuous-discrete conversion, there are many transform methods, i.e., Bilinear transform, forward Euler, backward Euler, etc. The users can choose the most suitable transform methods based on different application requirements.

2) Design of nth-Order $G_{imc}(s)$: Based on (7), it can be seen that $G_{\text{imc}}(s)$ possesses the low-pass filter characteristic to achieve the zero-speed steady-state error between ω_m and $\hat{\omega}_m$. Furthermore, $[1-G_{\text{imc}}(s)]\frac{\overline{K_t}i_q}{\overline{J}s}$ means the acceleration term and owns high-pass filter characteristic. In this case, the nth-order ($n \in \mathbb{Z}^+$) $G_{\text{imc}}(s)$ can be designed as

$$G_{\text{imc}}(s) = \frac{\frac{n(n-1)}{2}\omega_{\text{ob}}^{n-2}s^2 + n\omega_{\text{ob}}^{n-1}s + \omega_{\text{ob}}^n}{(s+\omega_{\text{ob}})^n} \tag{8}$$

where ω_{ob} denotes the undamped natural frequency related to the universal instantaneous IMC observer dynamic response bandwidth. The small value of ω_{ob} leads to the slow dynamic response for the acquisition of $\hat{\omega}$ under changeable external load-torque disturbances, but the magnitude of the measured noises is also reduced and the estimated speed becomes smooth. The speed tracking error transfer function $E(s)$ between $\hat{\omega}(s)$ and $\omega_m(s)$ can be expressed as

$$\begin{aligned}E(s) &= [G_{\text{imc}}(s)-1]\,\omega_m(s) \\ &= \frac{(s+\omega_{\text{ob}})^n - \frac{n(n-1)}{2}\omega_{\text{ob}}^{n-2}s^2 + n\omega_{\text{ob}}^{n-1}s + \omega_{\text{ob}}^n}{(s+\omega_{\text{ob}})^n}\omega_m(s).\end{aligned} \tag{9}$$

Employing the final value theorem, the speed steady-state error can reach to zero under the acceleration input speed $\omega_m(s) = \frac{c}{s^3}$ (constant acceleration c). The constant coefficient, the coefficient of s, and the coefficient of s^2 must be same as in the numerator and in the denominator in $G_{\text{imc}}(s)$, if the IMC observer cannot satisfy the zero speed steady-state error under acceleration input speed $\omega_m(t) = \frac{c}{2}t^2$. Substituting (8) into (7), the nth-order universal instantaneous IMC speed observer can be established. When $n=3$, the third-order $G_{\text{imc}}(s)$ is expressed as $\frac{3\omega_{\text{ob}}s^2+3\omega_{\text{ob}}^2s+\omega_{\text{ob}}^3}{(s+\omega_{\text{ob}})^3}$. Actually, it is noticeable that the third-order IMC speed observer model is completely same as the instantaneous speed observer of (4) (see, e.g., [8], [27], and [28]).

Remark 2: The universal instantaneous IMC speed observer can not only estimate the speed but also predict the load-torque disturbances T_l. The transfer function between $\hat{T}_l$ and T_l can be expressed as $\hat{T}_l(s) = \frac{\omega_{\text{ob}}^n}{(s+\omega_{\text{ob}})^n}T_l(s)$. Based on (7) and (8), the

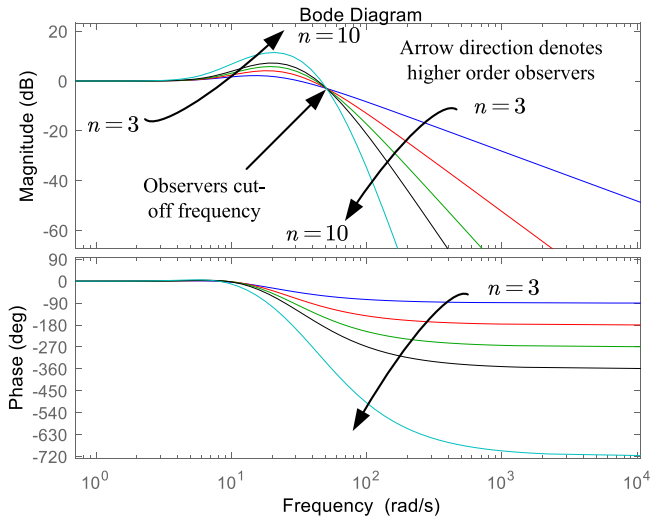

Fig. 3. Different order number $G_{\text{imc}}(s)$ transfer functions Bode comparison.

load-torque disturbance $\hat{T}_l$ can be obtained as follows:

$$\hat{T}_l(s) = \frac{\omega_{\text{ob}}^n s(\hat{\omega}_m - \theta_m s)}{(s+\omega_{\text{ob}})^n - \frac{n(n-1)}{2}\omega_{\text{ob}}^{n-2}s^2 + n\omega_{\text{ob}}^{n-1}s + \omega_{\text{ob}}^n}. \quad (10)$$

3) Analysis of High-Order Instantaneous IMC Speed Observer: Generally, without utilizing a sensorless technique, PMSM stator currents $\mathbf{i}_{dq}$ and position angle θ_m need to be measured, where both measurement parts can induce quantization noises (δ_{i_q} and δ_{θ_m}). Take the noises into account, and (7) can be rearranged as

$$\hat{\omega}_m = [1 - G_{\text{imc}}(s)] \overbrace{\frac{\overline{K_t}(i_q + \delta_{i_q})}{\overline{J}s}}^{\text{Term1}} + G_{\text{imc}}(s) \overbrace{s(\theta_m + \delta_{\theta_m})}^{\text{Term2}}. \quad (11)$$

In (11), it can be seen that Term1 is related to the integral of $i_q + \delta_{i_q}$, while Term2 is related to the derivative of $\theta_m + \delta_{\theta_m}$. As a result, it is noticeable that δ_{θ_m} can induce much more noises than δ_{i_q} for the acquisition of the evaluated speed since there exists a differential part in Term2. In order to suppress the high frequency δ_{θ_m} in Term2, a higher order transfer function $G_{\text{imc}}(s)$ should be preferred. This is a significant reason for designing high-order IMC speed observers. However, the stability of the IMC observers will be deteriorated with the increase in n, which is one of the limitations for higher order observers. The reason behind this is that the zero of $G_{\text{imc}}(s)$ is necessary to be designed to guarantee the zero-speed steady-state error between ω_m and $\hat{\omega}_m$ and can unavoidably induce the estimated speed overshoot phenomenon. The zero location effect on $G_{\text{imc}}(s)$ will be further amplified with the increase in n. In order to illustrate clearly, several different order number $G_{\text{imc}}(s)$ Bode comparison is shown in Fig. 3. In this graph, the blue, red, green, black, and cyan lines denote the third ($n = 3$), fourth ($n = 4$), fifth ($n = 5$), sixth ($n = 6$), and tenth ($n = 10$) order observers Bode plot, respectively. The instantaneous IMC observer cutoff frequency is set as the same value (50 rad/s) to make sure that the speed dynamic response is the same. It can be seen that although the magnitude of the high-frequency quantization noises can be further suppressed with the increase in n, there exists certain more than 0-dB magnitude below the value of the cutoff frequency, which means that the estimated speed overshoot occurs at a dynamic state. The value of the estimated speed overshoot will be increased with the increase in n. Furthermore, the phase margin of the IMC observers is gradually reduced with the increase in n. The phase margins ϕ_m of the IMC observers ($n = 3, n = 4, n = 5, n = 6, n = 10$) are 71.2°, 43.5°, 31.9°, 25.6°, and 15.8°, respectively. The higher the value of ϕ_m, the better the robustness of the IMC observer. In this case, the nth-order number selection should depend on the desired robustness of practical systems. In addition, the calculation is another barrier for high-order observer applications. Therefore, there is a tradeoff selection between the high- and low-order observers.

4) Digital Implementation of the IMC Speed Observer: Substituting (8) into (7), the continuous-discrete conversion transform can be employed to achieve the digital implementation of the universal instantaneous IMC speed observers.

Setting the fourth-order IMC speed observer as an example, substituting (8) into (7), $G_{\text{imc}}(s)$ can be expressed as $\frac{6\omega_{\text{ob}}^2 s^2 + 4\omega_{\text{ob}}^3 s + \omega_{\text{ob}}^4}{(s+\omega_{\text{ob}})^4}$ and the estimated speed can be obtained. In this article, backward Euler ($\frac{1}{s} \to \frac{T_s z}{z-1}$) will be employed to transform the transfer function from the s domain to the z domain

$$\begin{cases} \hat{\omega}_{m1}(z) = \frac{\theta_m(z) - \theta_m(z)z^{-1}}{T_s} \\ \hat{\omega}_{m3}(z) = \frac{\hat{\omega}_{m3}(z)z^{-1}\Gamma + \left[\frac{\overline{K_t} T_s i_q(z)}{\overline{J}} - \hat{\omega}_{m1}(z)(1-z^{-1})\right]\Delta}{a_1} \\ \hat{\omega}_m(z) = \hat{\omega}_{m1}(z) + \hat{\omega}_{m3}(z) \end{cases} \quad (12)$$

where $\Gamma = a_2 + a_3 z^{-1} + a_4 z^{-2} + a_5 z^{-3} + z^{-4}$ and $\Delta = b_1 + b_2 z^{-1} + b_3 z^{-2} + b_4 z^{-3} + z^{-4}$. After determining the related coefficients as listed in Appendix A, the digital implementation of the fourth-order instantaneous IMC speed observer can be carried out in digital control systems.

B. Proposed Speed Controller With an Active Damping Structure Considering a Current Loop Model

1) Proposed Speed Controller Structure Design: To pursuit the speed control high performance, including the speed dynamic response, disturbance rejection, measurement noise suppression, and system robustness, a novel speed controller with an active damping structure considering a current loop model is proposed herein, as shown in Fig. 4. An adjusted robust coefficient α is designed in the proposed speed controller structure. The proposed speed controller mainly includes four parts, i.e., active damping structure, anti-integral windup, PI-type regulator considering current loop, and tuned robust α. The proposed open-loop speed transfer function G_{ols3} is presented as follows:

$$\begin{cases} G_{\text{ols3}}(s) = \frac{\overline{J}\omega_{\text{spd}}^2(\frac{s}{\omega_c}+1)}{s} \frac{\omega_c}{s+\omega_c} \alpha \frac{K_t}{\overline{K_t}} \frac{1}{J(s+2\omega_{\text{spd}}\alpha\frac{\overline{J}K_t}{J\overline{K_t}})} \\ K_{p3} = \frac{\overline{J}\omega_{\text{spd}}^2}{\omega_c}, \quad K_{i3} = \overline{J}\omega_{\text{spd}}^2, \quad \alpha = \frac{J\overline{K_t}}{K_t\overline{J}}. \end{cases} \quad (13)$$

Remark 3: The active damping structure and the PI-type regulator are employed to establish a second-order closed-loop

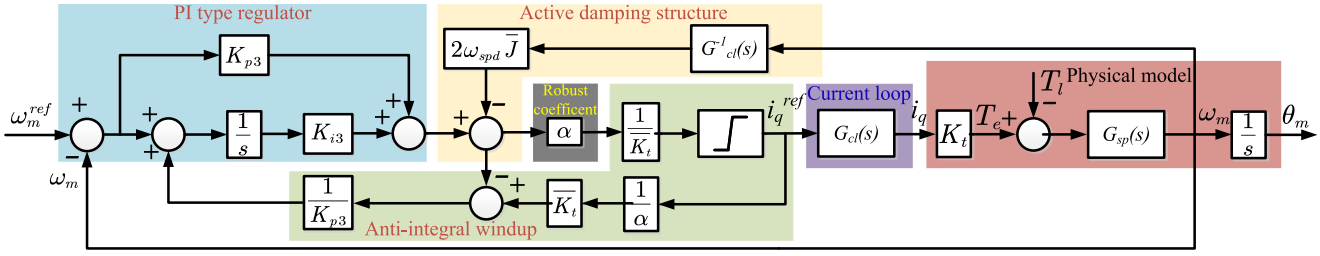

Fig. 4. Transfer function block diagram of the proposed speed controller.

speed system, which has better high-frequency measurement noise suppression, compared with the first-order closed-loop speed system [23]. It should be noted that the value of α is initially set to 1 without PMSM parameter mismatch. The value of α can also be determined by parameter identification techniques, i.e., recursive least squares, offline parameter lookup table, offline parameter curve fitting, model reference adaptive parameter, extended Kalman filter, invasive injection techniques, etc. Without obtaining the actual PMSM parameters, α can be theoretically adjusted to improve the speed overall system robustness, and the tuning guidance is presented in the next subsection in detail. With respect to the integrator windup issue, there are several anti-integral windup techniques [3], [32], [33], and back calculation anti-integral windup is employed herein [32].

2) Proposed Speed Controller Performance Evaluation: In this subsection, the dynamic response performance, load-torque disturbance rejection, and measurement noise suppression of the proposed speed controller will be evaluated compared with PI-type and ADRC speed controllers. Before the evaluation, several conditions need to be assumed to reduce the complexity of the analysis, i.e., $K_t = \overline{K_t}, J = \overline{J}$ resulting in $\alpha = 1$, the closed-loop current transfer function (2) is considered, and the third-order instantaneous speed observer is employed in the ADRC speed controller [8], [27], [28].

In terms of the dynamic response performance evaluation, according to (13) the speed closed-loop transfer functions of the three speed controllers can be, respectively, expressed as

$$\begin{aligned} G_{\text{cls1}}(s) &= \frac{(2\omega_{\text{spd}}s + \omega_{\text{spd}}^2)\omega_c}{s^3 + s^2\omega_c + 2\omega_c\omega_{\text{spd}}s + \omega_{\text{spd}}^2\omega_c} \\ G_{\text{cls2}}(s) &= \frac{\omega_c\omega_{\text{spd}}}{s^2 + \omega_c s + \omega_c\omega_{\text{spd}}} \\ G_{\text{cls3}}(s) &= \frac{\omega_{\text{spd}}^2}{(s+\omega_{\text{spd}})^2} \end{aligned} \tag{14}$$

where $G_{\text{cls1}}(s), G_{\text{cls2}}(s)$, and $G_{\text{cls3}}(s)$ denote the PI-type, ADRC, and proposed speed controllers, respectively. It can be seen that the undesired coupling between ω_c and ω_{spd} occurs in the pole location of the first two (14). In G_{cls2}, there exists a speed overshoot phenomenon because the second-order system is underdamped under the condition that $\omega_{\text{spd}} > \frac{\omega_c}{4}$. On the contrary, there is no speed overshoot under the condition that $\omega_{\text{spd}} \leq \frac{\omega_c}{4}$, but the dynamic response speed is determined by both ω_{spd} and ω_c. This is a reason why the value of the speed loop bandwidth needs to be set smaller several times than the current loop bandwidth. In G_{cls1}, the zero location also induces a certain speed overshoot. Nevertheless, G_{cls3} can only be determined by ω_{spd} based on (14) and is fully critically damped under different values of the current loop bandwidth.

In the field of the load-torque disturbance rejection evaluation, an effective performance measure is to employ an integrated error ζ [32], which can be presented in (15). A load-torque step $T_l(s) = \frac{\kappa}{s}$ is applied herein, and $G_{Tl1}(s), G_{Tl2}(s)$, and $G_{Tl3}(s)$, respectively, denote the PI-type, ADRC, and proposed speed controllers

$$\begin{aligned} \zeta_1 &= \int_0^\infty (\omega_m^{\text{ref}} - \omega_m)d\tau = \lim_{s\to 0} T_l(s)G_{Tl1}(s) \\ &= \lim_{s\to 0} \frac{\kappa\left[s^3 + s^2\omega_c\right]}{s^2(s^3 + s^2\omega_c + 2\omega_c\omega_{\text{spd}}s + \omega_{\text{spd}}^2\omega_c)} = \frac{\kappa}{\omega_{\text{spd}}^2} \\ \zeta_2 &= \lim_{s\to 0}\left[\frac{\omega_{\text{ob}}^3}{(s+\omega_{\text{ob}})^3}\frac{\omega_c}{s+\omega_c} - 1\right]\frac{\kappa(s^2 + \omega_c s)}{s^4 + \omega_c s^3 + \omega_c\omega_{\text{spd}}s^2} \\ &= \frac{\kappa(\omega_{\text{ob}} + 3\omega_c)}{\omega_{\text{ob}}\omega_c\omega_{\text{spd}}} \\ \zeta_3 &= \lim_{s\to 0}\frac{\kappa}{(s+\omega_{\text{spd}})^2} = \frac{\kappa}{\omega_{\text{spd}}^2}. \end{aligned} \tag{15}$$

In (15), it can be seen that the smaller the value of ζ, the better the disturbance rejection performance. In the PI-type and proposed speed controllers, ω_{spd} is the only coefficient for the disturbance rejection performance, and the value should be set largely to enhance disturbance rejection. It can be known that the dynamic response and disturbance rejection can be both enhanced by increasing the value of ω_{spd}. Thus, ω_{spd} can also stand for the external disturbance rejection coefficient in the proposed structure. Conversely, $\omega_c, \omega_{\text{spd}}$, and ω_{ob} all affect the load-torque disturbance rejection performance in the ADRC speed controller. Increasing the value of ω_c can enhance the disturbance rejection, which means that there exists the unavoidable coupling between ω_c and disturbance rejection. The other demerit of the ADRC speed controller is that increasing the value of ω_{ob} can amplify the speed measurement noise from the speed observer based on (4). It should be noted that although ζ is employed, the absolute of the values is different, i.e., the total sum ζ of negative and positive values of $\omega_m^{\text{ref}} - \omega_m$ is the same, but the disturbance rejection performance is different, as explained in Fig. 5. Setting an example in Fig. 5, although $\zeta_1 = \zeta_3$ ($\mathbf{H1} + \mathbf{H2} + \mathbf{H3} = \mathbf{H4}$), the negative value exists in

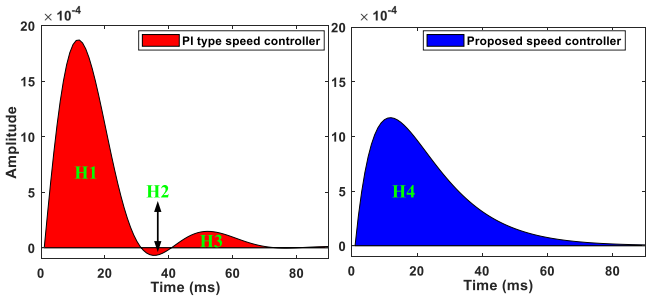

Fig. 5. Step response of $G_{Tl1}(s)$ and $G_{Tl3}(s)$ with the same coefficients ($\omega_{\text{spd}} = 100\pi\text{rad/s}$ and $\omega_c = 200\pi\text{rad/s}$).

G_{Tl1}, resulting in $|\zeta_1| > |\zeta_3|$ ($|\mathbf{H1}| + |\mathbf{H2}| + |\mathbf{H3}| > |\mathbf{H4}|$). In this case, the best disturbance rejection is the proposed speed controller.

For the measurement noise suppression evaluation, it should be assumed that the measured speed from the position sensor contains both parts, i.e., the measured speed ω_m and measured speed noises δ_{ω_m}. Consequently, the measurement noise transfer function between the measured speed noises δ_{ω_m} and the measured speed ω_m of the PI-type, ADRC, and proposed speed controllers can be, respectively, expressed as the negative term of (14), also called complementary sensitivity function. Thus, based on (14), a coupling issue between ω_c and measurement noise suppression exists in the PI-type and ADRC speed controllers, while the measurement noise suppression of the proposed speed controller can only be determined by ω_{spd}. The measurement noise suppression can be enhanced with the reduction of ω_{spd}, and there is a tradeoff between the measurement noise suppression and dynamic response speed rate. However, compared with the first-order system $\frac{\omega_{\text{spd}}}{(s+\omega_{\text{spd}})}$, the second-order system $G_{\text{cls3}}(s)$ should have better measurement noise suppression performance under the same dynamic response performance condition.

3) Digital Implementation of the Proposed Speed Controller: Based on Fig. 4, the digital implementation of the proposed speed controller can be easily carried out. The forward Euler is employed to discretize and the digital format of the speed controller can be expressed as

$$\begin{cases} e_p(k) = \left[\omega_m^{\text{ref}}(k) - \omega_m(k)\right] K_{p3} \\ e_{ii}(k) = \omega_m^{\text{ref}}(k-1) - \omega_m(k-1) + e_A(k-1) \\ e_{io}(k) = e_{ii}(k) T_s K_{i3} + e_{io}(k-1) \\ \omega_1(k) = \frac{\omega_m(k) - \omega_m(k-1)}{\alpha T_s} + \omega_m(k) \\ i_{dq}^{\text{ref}}(k) = \frac{\alpha}{\overline{K_t}} \text{Sat}\left[e_p(k) + e_{io}(k) - 2\omega_{\text{spd}}\overline{J}\omega_1(k)\right] \\ e_A(k) = \frac{i_{dq}^{\text{ref}}(k)\frac{\overline{K_t}}{\alpha} - \left[e_p(k) + e_{io}(k) - 2\omega_{\text{spd}}\overline{J}\omega_1(k)\right]}{K_{p3}} \end{cases} \tag{16}$$

where the function $\text{Sat}(x)$ stands for the saturation function ($\text{Sat}(x) = l, \text{if } x > l; \text{Sat}(x) = -l, \text{if } x < -l; \text{Sat}(x) = x, \text{otherwise}$).

C. Digital Speed Control System Performance Evaluation

Combining with the proposed universal instantaneous IMC speed observer and the proposed speed controller, the proposed digital speed control system can be established. In this subsection, the fourth-order IMC speed observer is employed, and the corresponding coefficients, i.e., T_s and PMSM parameters, are consistent with that in the experiment part. Since the ZOH voltage latch and one-step control delay exist in the practical system, the digital speed control system in the z domain will be analyzed to reduce the unnecessary approximation in this article. Moreover, the effect of T_s on the overall system is significant, and the designed coefficients considering system robustness totally depend on the value of T_s. In this case, it is straightforward to theoretically design these coefficients based on the digital speed control system. The z-domain transfer function block diagram is shown in Fig. 6, where $G_{\text{zoh}}(z)$ is the current loop model transfer function. The speed open-loop transfer function $\text{G}_{\text{ols}}(z)$ of Fig. 6 can be expressed as

$$G_{\text{ols}}(z) = \frac{\overline{J}\omega_{\text{spd}}^2 T_s}{z-1} \frac{z-1+T_s\omega_c}{T_s\omega_c} \frac{\alpha K_t T_s G_{\text{zoh}}(z)}{\overline{K_t} J\left(z-1+2\omega_{\text{spd}}T_s\alpha\frac{\overline{J}K_t}{\overline{K_t}J}\right)}. \tag{17}$$

1) Current Loop Model Influence: Compared with other unmodeled models, i.e., measurement and anti-aliasing filters, and time delays resulting from analog/digital conversion, a current loop model is more significant for the overall system, especially under low current loop bandwidth [e.g., there exists the speed overshoot under $\omega_{\text{spd}} > \frac{\omega_c}{4}$ based on (14)]. Therefore, it is necessary to analyze the current loop model before designing the speed control system.

Currently, current controllers can be mainly divided into two types, namely, PI-type and predictive current controllers (see, e.g., [3]). In digital current loops, the ZOH voltage latch and one-step control delay should be considered. In the PI-type current controller scheme, the current loop model $G_{\text{zoh}}(z)$ can be expressed as

$$G_{\text{zoh}}(z) = \frac{\omega_c \mathbf{Z}\left\{\frac{s\mathbf{A}+\mathbf{B}}{s}\right\}(1-z^{-1})\mathbf{Z}\left\{\frac{G_{cp}(s)}{s}\right\}z^{-1}}{1+\omega_c \mathbf{Z}\left\{\frac{s\mathbf{A}+\mathbf{B}}{s}\right\}(1-z^{-1})\mathbf{Z}\left\{\frac{G_{cp}(s)}{s}\right\}z^{-1}}. \tag{18}$$

Based on the above equation, the PI-type current loop transfer function can be simplified as $G_{\text{zoh1}}(z) = \frac{T_s\omega_c}{z^2-z+T_s\omega_c}$. On the contrary, in the predictive current controller, since the $(k+1)$th instant current can be predicted based on the current instant (kth) measured voltage and current, the predictive current loop transfer function can be presented as $G_{\text{zoh2}}(z) = \frac{T_s\omega_c}{z-1+T_s\omega_c}$. $G_{\text{zoh1}}(z)$ and $G_{\text{zoh2}}(z)$ can be taken as a first- and second-order current loop system, respectively. Based on (17), the phase margin ϕ_m of the overall speed system with $G_{\text{zoh1}}(z)$ is smaller than that based on $G_{\text{zoh2}}(z)$ in Fig. 6. For example, setting ω_{spd} as $\frac{0.9}{T_s}$, ϕ_m of the overall speed system with $G_{\text{zoh1}}(z)$ is 32.5°, whereas $\phi_m = 61.7°$ occurs in the overall speed system with $G_{\text{zoh2}}(z)$ under the same model parameter and coefficient condition. Consequently, the predictive current controller is more suitable for the proposed digital speed control system. It should be noted that there may exist model parameter mismatch in the current loop, lookup table, or model-based DOB; adaptive parameter identification can be employed to handle for that, which is not focused on this article.

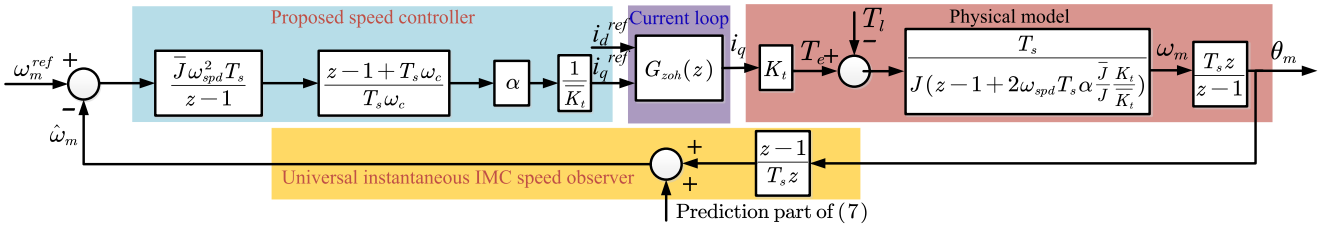

Fig. 6. z-domain transfer function block diagram of the proposed digital speed control system.

2) Design Guidance for ω_{spd} and α: Assume that the predictive current controller is employed in this article before illustration. In the speed loop, it can be known that both inaccurate parameters $\overline{K_t}$ and $\overline{J}$ can induce the system instability. Defining the term $\alpha\frac{\overline{J}K_t}{\overline{K_t}J}$ of (17) as χ, the speed closed-loop transfer function $G_{\text{cls}}(z)$ can be expressed as follows:

$$G_{\text{cls}}(z)=\frac{\chi\omega_{\text{spd}}^2T_s^2}{z^2+2(\chi\omega_{\text{spd}}T_s-1)z+\chi\omega_{\text{spd}}^2T_s^2-2\chi\omega_{\text{spd}}T_s+1}. \tag{19}$$

It can be seen that both ω_{spd} and α can affect the system robustness. According to (19), the pole location can be presented as

$$z_{01}=\begin{cases}1-\omega_{\text{spd}}T_s(\chi\pm\sqrt{\chi-\chi^2}\text{j}), & \chi\in(0,1)\\ 1-\omega_{\text{spd}}T_s, & \chi=1\\ 1-\omega_{\text{spd}}T_s(\chi\pm\sqrt{\chi^2-\chi}), & \chi>1\end{cases} \tag{20}$$

where j denotes the imaginary part. Without $\overline{J}$ and $\overline{K_t}$ parameter mismatch, it can be seen that ω_{spd} can be determined by a unit circle in the z domain (the stability criterion is $|z|\le 1$) as $\omega_{\text{spd}}\in[0,\frac{2}{T_s}]$. The optimum ω_{spd} design should meet as $\omega_{\text{spd}}\in[0,\frac{1}{T_s}]$ to avoid the speed overshoot phenomenon. The design guidance of ω_{spd} can be based on the desired speed system dynamic response, and the speed dynamic response becomes fast with the increase in ω_{spd}, and *vice versa*. ω_{spd} can also be computed by the desired setting time t_s ($t_s=\frac{4}{\omega_{\text{spd}}}$) and can be expressed as $\frac{4}{t_s}$ for 2% or $\frac{3}{t_s}$ for 5%, respectively.

Initially, the value of α is set to 1. However, the desired speed performance with the computed ω_{spd} cannot be achieved when $\overline{J}$ and $\overline{K_t}$ parameter mismatch occurs in practical systems. In this case, the actual dynamic response is inconsistent with the designed dynamic response, and users can only tune α to achieve the designed dynamic response without changing the determined ω_{spd}. Therefore, the design guidance for tuning α is presented in this subsection. α is set to 1 initially, and users will see the speed dynamic response under the determined ω_{spd} in real time. Based on this criterion, the determined ω_{spd} can reflect the actual speed dynamic response performance. For example, setting the small value of ω_{spd} in the speed controller, the speed dynamic response gets slow. When there exists the speed overshoot, χ is located in (0,1) due to the involvement of j, and α should be increased manually until the speed overshoot is missing. When the speed dynamic response gets much slow and cannot match the setting value of ω_{spd}, χ is located in $(1,+\infty)$ because of the dominant pole is $1-\omega_{\text{spd}}T_s(\chi+\sqrt{\chi^2-\chi})$. It can be known that the value of the dominant pole is located in $(0,1-\omega_{\text{spd}}T_s)$, which means that the speed bandwidth is reduced. In this case, α needs to be decreased manually until the dynamic response speed gets recovered back. When the speed is unstable, χ should be located in $(1,+\infty)$. The reason is that the following condition may happen as $|1-\omega_{\text{spd}}T_s(\chi+\sqrt{\chi^2-\chi})|>1$ with the large value of χ. In order to stabilize the system, α also needs to be decreased manually.

3) Speed Loop Parameter Robustness: Regarding the speed loop parameter robustness evaluation, the value of the robust coefficient α needs to be set to 1. It can be seen that the speed control system stability mainly depends on the value of ω_{spd} in (20). χ stands for the parameter robustness, and a larger value of χ means the better parameter robustness and *vice versa*. Based on the discrete-time stability criteria, χ needs to meet the following term based on (19):

$$\frac{\overline{J}K_t}{\overline{K_t}J}=\chi\in\left(0,0.5+\sqrt{0.25+(\frac{2}{\omega_{\text{spd}}T_s}-1)^2}\right]. \tag{21}$$

It can be seen that the range of χ is reduced with the increase in ω_{spd} based on (21), and *vice versa*. There is a tradeoff between dynamic response and parameter robustness. Based on (20), when $\frac{\overline{J}}{\overline{K_t}}\le\frac{J}{K_t}$, the instability never occurs under $\omega_{\text{spd}}\in[0,\frac{1}{T_s}]$. On the contrary, when $\frac{\overline{J}}{\overline{K_t}}>\frac{J}{K_t}$, the instability may occur since the pole location of $G_{cl}(z)$ can be out of the unit circle.

With respect to the parameter robustness analysis of the proposed IMC speed observer, it can be seen that the parameter disturbances caused by $\overline{J}$ and $\overline{K_t}$ can also affect the IMC speed observer robustness based on (7). In order to give an investigation on tolerance degree of the parameter mismatch, the worst system robustness is defined as the phase margin $\phi_m<30^\circ$ in this article. Therefore, the acceptable parameter mismatch range for the third- and fourth-order IMC speed observers is $\frac{\overline{J}}{\overline{K_t}}>\frac{J}{5K_t}$ and $\frac{\overline{J}}{\overline{K_t}}>\frac{J}{1.5K_t}$, respectively. It can be seen that the third-order IMC speed observer can have better parameter robustness than that of the fourth-order IMC speed observer.

4) Speed Performance Consistency Between the Controller and the Observer Under Parameter Uncertainty: To analyze the speed performance consistency of the controller and the observer under parameter uncertainty ($\overline{K_t}$ and $\overline{J}$), the value of α also needs to be set to 1. In the speed observer, based on (7), it can be easily found that the estimated speed $\hat{\omega}$ under the

parameter mismatch condition that $\frac{\overline{J}}{\overline{K_t}} < \frac{J}{K_t}$ is larger than the estimated speed ω without parameter mismatch. Consequently, the speed dynamic response becomes faster under the parameter uncertainty. When $\frac{\overline{J}}{\overline{K_t}} > \frac{J}{K_t}$, the estimated speed $\hat{\omega}$ is smaller than the estimated speed ω without parameter mismatch, and hence, the speed dynamic response becomes slow. On the other hand, in the ADRC speed controller, the speed open-loop transfer function without considering the current loop can be obtained as $\frac{\chi\omega_{\text{spd}}}{s}$ based on (5) and (6). Therefore, the closed-loop transfer function in the z domain based on the forward Euler ($\frac{1}{s} \to \frac{T_s}{z-1}$) can be expressed as $\frac{\chi\omega_{\text{spd}}T_s}{z-1+\chi\omega_{\text{spd}}T_s}$. Based on the transfer function, when $\frac{\overline{J}}{\overline{K_t}} < \frac{J}{K_t}$, $\chi \in (0,1)$, the speed dynamic response of the ADRC speed controller gets slower. It can be easily found that the ADRC speed controller cannot get the consistent speed dynamic performance with the speed observer. On the contrary, in the proposed speed controller, when $\frac{\overline{J}}{\overline{K_t}} < \frac{J}{K_t}$, the speed overshoot will occur based on (20), while the slow speed dynamic response will occur under $\frac{\overline{J}}{\overline{K_t}} > \frac{J}{K_t}$. Therefore, the proposed controller has the consistent speed dynamic response with the speed observer.

In other words, it is straightforward to tune α for improving the speed dynamic response performance under the speed loop parameter uncertainty in the proposed digital speed control system. The proposed speed controller is much more suitable for the IMC speed observer, compared with the ADRC speed controller. According to the speed performance consistency merit, α can be added in the IMC observer (7), which can be expressed as

$$\hat{\omega}_m = [1 - G_{\text{imc}}(s)]\left(\frac{\overline{K_t} i_q}{\alpha \overline{J} s} - \theta_m s\right) + \theta_m s. \tag{22}$$

For example, when the condition that $\frac{\overline{J}}{\overline{K_t}} < \frac{J}{K_t}$ happens, α can be manually increased based on the actual dynamic speed response, which can reduce the parameter mismatch effect on the proposed speed observer based on (22). On the contrary, when $\frac{\overline{J}}{\overline{K_t}} > \frac{J}{K_t}$, α can be manually reduced, and hence, the disturbance caused by the parameter mismatch effect on the proposed speed observer based on (22) is decreased. Overall, because of the speed performance consistency, the proposed overall speed system performance can be immune to the parameter mismatch effect through suitably adjusting α.

IV. Experimental Result Verification

A. PMSM Test Rig Setup

The PMSM test rig is constructed as shown in Fig. 7, where two XCUBE controllers (the main MCU is TMSF320F28377d) are employed as the drive and load control system. The drive and load inverters are consisted of the silicon carbide (SiC) power modules and intelligent power modules based on an insulated-gate bipolar transistor. The oscilloscope is the high-performance Lecroy MDA8058HD. The 12-V auxiliary power supply is used for energizing the control system. The PMSM and controller parameters are listed in Table I.

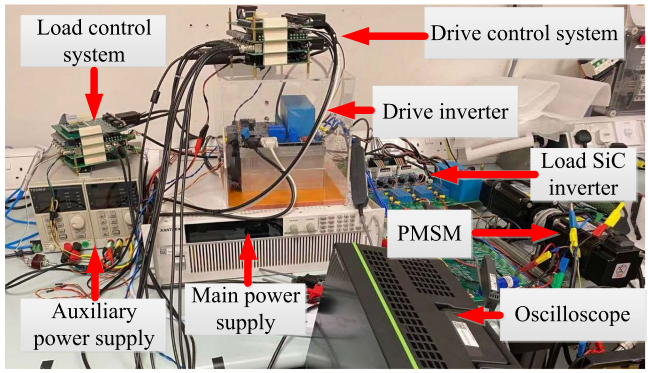

Fig. 7. PMSM test rig setup.

TABLE I
PMSM and Controller Parameters

Parameters	Value	Unit	Parameters	Value	Unit
Stator Resistance (R_s)	1.1	Ω	Flux Linkage (ψ_m)	0.092	Wb
D-axis Inductance (L_d)	5.7e-3	H	Q-axis Inductance (L_q)	5.7e-3	H
Rated Current (I_N)	4.2	A	VSI Deadtime (t_d)	2.5	μs
Torque Constant (K_t)	0.552	Nm/A	Inertia (J)	4.53e-4	kg m^2
Control Period (T_s)	100	μs	ADC Resolution	12	bit
Machine Pole Pairs (p)	4		Encoder Resolution	2500	PPR

B. Speed Measurement Performance Evaluation

In order to evaluate the speed measurement performance, the ADRC speed controller is adopted as the speed controller part. Four types of the speed measurement method will be compared, i.e., M method combined with the first-order low-pass filter (Method1) where the low-pass filter cutoff frequency is 100 Hz, the instantaneous speed observer based on the angle error (Method2) [8], the proposed third-order IMC speed observer (Method3), and the proposed fourth-order IMC speed observer (Method4). The M method is a speed measurement approach and can be expressed as

$$\hat{\omega}_m(k) = \frac{\theta_m(k) - \theta_m(k-1)}{T_s} \tag{23}$$

where k is the sample number index. It should be noted that there is a slight phase lag between the reference speed and the measured speed due to the limited speed loop bandwidth. The experimental results for quantization noise suppression and high-order parameter robustness will be carried out in this subsection.

1) Quantization Noise Suppression: ω_c and ω_{spd} are set to $2\pi 500$ and $2\pi 200\text{rad/s}$, respectively. It should be noted that setting the same value of the cutoff frequency in different order number observers, ω_{ob} should be different. For example, ω_{ob} of Method2 and Method3 is set to 1.962 times $2\pi 50\text{rad/s}$, while ω_{ob} of Method4 needs to be set to 2.3 times $2\pi 50\text{rad/s}$. In this case, the three speed observers can have the same estimated speed dynamic response based on -3-dB cutoff frequency definition. The sinusoidal waveform $[f_{\text{sin}}(t) = 100 + 50\sin(30\pi t)]$ is considered as the speed reference. Fig. 8 shows the measured and reference speed performance comparison. It can be seen that more delay lag and slight speed overshoot exists in Method1,

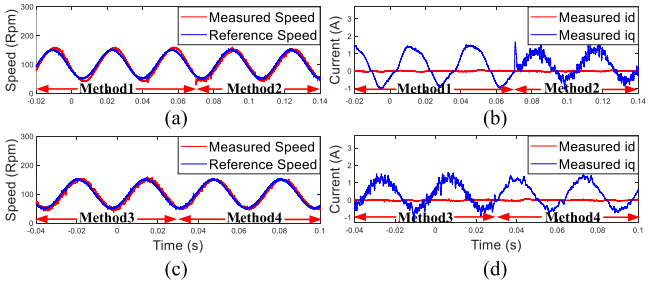

Fig. 8. Quantization noise suppression performance of four methods. (a) and (b) From Method1 switch to Method2. (c) and (d) From Method3 switch to Method4.

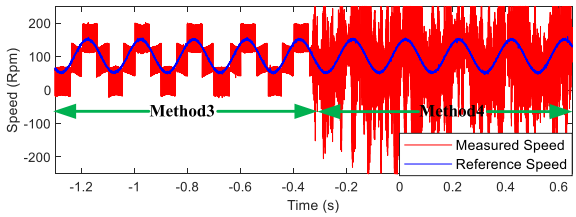

Fig. 9. Estimated speed performance comparison with the large values of ω_{ob} under $\frac{\overline{J}}{K_t} = \frac{J}{2K_t}$ parameter mismatch.

but the measured speed waveform is much more smoother than Method2 and Method3. Compared with Method3, the measured speed of Method4 is smoother, which can validate that the quantization noise is further reduced with the fourth-order speed IMC observer.

2) High-Order Parameter Robustness: First, to validate the conclusion that higher order IMC observer has worse robustness, ω_c and ω_{spd} are set to $2\pi 300$ and $2\pi 50\text{rad/s}$, respectively. In order to keep the same estimated speed dynamic response, ω_{ob} of Method3 and Method4 is set to 1.962 and 2.3 times $2\pi 260\text{rad/s}$, respectively. The sinusoidal waveform $[f_{\sin}(t) = 100 + 50\sin(5\pi t)]$ is considered as the speed reference. With the PMSM nominal parameter mismatch of the controller condition ($\frac{\overline{J}}{K_t} = \frac{J}{2K_t}$), the estimated speed performance of Method3 and Method4 can be shown in Fig. 9. It can be seen that more high-frequency noises occur in Method4 and the system robustness is deteriorated, which means that the estimated speed cannot be obtained accurately compared with Method3 with the large value of ω_{ob}. When setting the small value of ω_{ob}, the high-frequency noises of Method4 can be eliminated, and hence, it can be concluded that the value of ω_{ob} can affect the robustness of the proposed observers. Second, to investigate the acceptable parameter mismatch range for Method3 and Method4, the related test is carried out, and it is found that the acceptable parameter mismatch range for Method3 and Method4 is $\frac{\overline{J}}{K_t} > \frac{J}{6.7K_t}$ and $\frac{\overline{J}}{K_t} > \frac{J}{2.5K_t}$, respectively, with small values of ω_{ob}, where the values of ω_{ob} of Method3 and Method4 are 1.962 and 2.3 times $2\pi 30\text{rad/s}$, respectively. Third, keeping the small value of ω_{ob}, the estimated speed performance comparison of Method3 and Method4 under parameter mismatch $\frac{\overline{J}}{K_t} = \frac{J}{5K_t}$ is carried out in Fig. 10. It can be seen that the estimated speed performance of

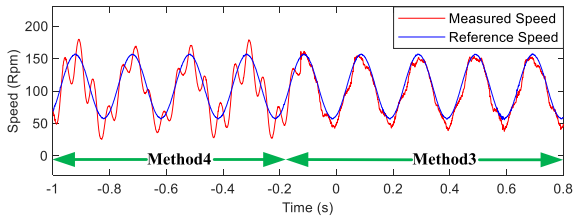

Fig. 10. Estimated speed performance comparison with the small values of ω_{ob} under $\frac{\overline{J}}{K_t} = \frac{J}{5K_t}$ parameter mismatch.

Method4 is worse than that in Method3. Overall, according to the above tests, it can be validated that the parameter robustness of the IMC speed observer is deteriorated with the increase in n, and both the parameter mismatch and ω_{ob} can affect the IMC speed observer robustness.

C. Speed Controller Performance Evaluation

To evaluate the speed controller performance, the proposed fourth-order IMC speed observer is employed herein, and three types of speed controller will be compared, namely, the ADRC with the fourth-order DOB, conventional PI-type, and proposed speed controllers, where the value of α is set to 1.

1) Dynamic Response: ω_{spd} of the ADRC, PI-type, and proposed speed controllers should be, respectively, set to $2\pi 50\text{rad/s}$, about 0.5 times $2\pi 50\text{rad/s}$, and 1.554 times $2\pi 50\text{rad/s}$ to obtain the approximately same value of the cutoff frequency of the speed closed-loop system. The value of 1-N· m torque is set in the load system. When ω_c is set to $2\pi 350\text{rad/s}$ ($\omega_{\text{spd}} < \frac{\omega_c}{4}$), the current loop can be neglected in terms of the speed dynamic response, which is shown in Fig. 11(a), (c), and (e). It can be seen that the speed dynamic response is almost the same in ADRC and proposed speed controllers, whereas the speed overshoot occurs in the PI-type speed controller because the unavoidable zero exists in the speed closed-loop transfer function. In order to testify the controller performance under the condition that $\omega_{\text{spd}} > \frac{\omega_c}{4}$, increasing the speed loop bandwidth, setting the same speed loop and the cutoff frequency in the three speed controllers, and reducing the value of ω_c to $2\pi 100\text{rad/s}$, the speed dynamic response comparison is shown in Fig. 11(b), (d), and (f). It can be seen that the better speed dynamic response without speed overshoot exists in the proposed speed controller compared with the other speed controllers. In addition, it can be seen that the maximum q-axis current of the proposed speed controller is the smallest, which can save more power in speed control systems. It should be noted that the maximum q-axis current limitation is set to 12 A to make sure that the speed control system is a linear system.

2) External Load-Torque Disturbance Rejection: In order to compare the external load-torque disturbance rejection, the dynamic response performance should be kept the same. In addition, $4\omega_{\text{ob}} = \omega_{\text{spd}}$ should be set to obtain the same disturbance rejection because the fourth-order DOB based on (15) is employed in the ADRC speed controller. The rated value of load torque is carried out as an external load torque, and the reference speed keeps the constant value 500 r/min. Fig. 12

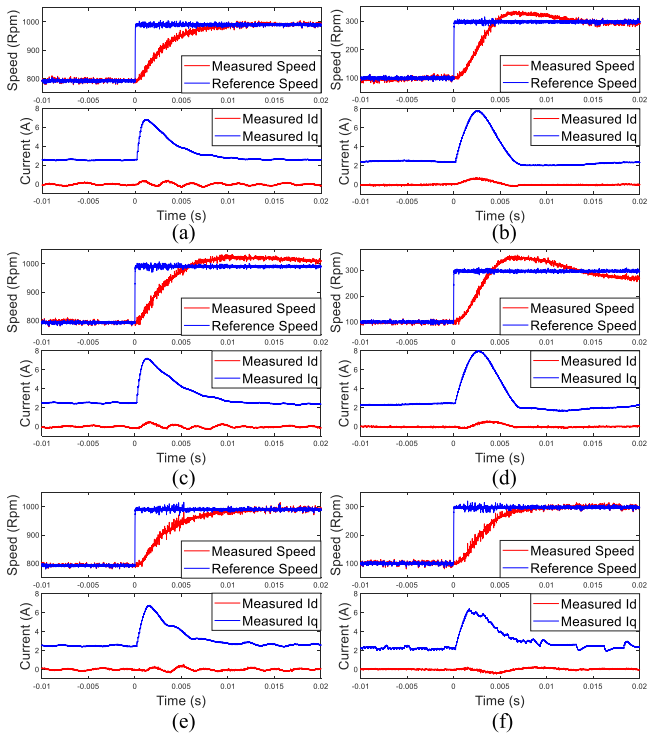

Fig. 11. Speed dynamic response performance comparison of three speed controllers. (a) and (b) ADRC speed controller. (c) and (d) PI-type speed controller. (e) and (f) Proposed speed controller.

shows the external disturbance rejection comparison of the three speed controllers. It can be seen that there are large noises in the measured speed of the ADRC speed controller since $4\omega_{\text{ob}}$ is set to enhance the load-torque disturbance rejection; meanwhile, the measured speed is affected by $4\omega_{\text{ob}}$ and the waveform becomes rough. There is a tradeoff between the disturbance rejection and the measured speed waveform. In addition, since ω_c can reduce the disturbance rejection in the ADRC speed controller based on (15), the speed overshoot is larger than other controllers. In the PI-type speed controller, based on the theoretical analysis of Fig. 5, the speed overshoot is slightly larger than that in the proposed speed controller. Therefore, the best disturbance rejection is the proposed speed controller among the three speed controllers.

3) Speed Measurement Noise Suppression: In order to make a fair comparison, the M method with the first-order low-pass filter is employed in the speed measurement and ω_c is all set to $2\pi 500\text{rad/s}$. Since the speed measurement noise is complimentary with the speed closed-loop system dynamic response, the speed dynamic response cutoff frequency should be set to the same value in the ADRC and proposed speed controllers. Fig. 13 shows the speed measurement noise suppression comparison under low-speed condition. It can be seen that the measured speed noise is reduced from the ADRC to proposed speed controllers. In addition, the speed measurement noise suppression comparisons under 700 and 1500 r/min speed conditions are carried out in Fig. 14. It can be seen that the measurement noises are also decreased under 700 r/min speed condition, but there is almost the same measured speed performance under 1500 r/min speed condition. The main reason behind this is that the magnitude of the measured noises is reduced under rated speed condition. In this case, the effect of measured noises on the overall system can be neglected under rated speed condition. Based on the above test results, it can be concluded that the proposed speed controller has better measurement noise suppression than that in the ADRC speed controller.

D. Digital Speed Control System Performance Evaluation

1) Parameter Robustness: In order to validate the system parameter robustness, the ADRC speed control system and the proposed speed control system will be carried out. It should be noted that the speed dynamic response should remain the same in the two speed control systems, and the value of α is set to 1. The fourth-order IMC speed observer is employed herein, and ω_{ob} is set to $2\pi 50\text{rad/s}$. ω_c is all set to $2\pi 300\text{rad/s}$. When $\frac{\overline{J}}{K_t} = \frac{J}{4K_t}$ $(\chi \in (0,1))$, the speed dynamic response has overshoot in the both speed control systems, which is shown in Fig. 15. It can be found that the smaller amplitude of the speed overshoot is in the proposed speed control system. On the contrary, Fig. 16 shows the speed dynamic response under the speed loop parameter mismatch $\frac{\overline{J}}{K_t} = \frac{4J}{K_t}$ $(\chi > 1)$. It can be seen that the speed dynamic response becomes slower in the two speed control systems, and there exists fluctuated speed waveform in the ADRC speed control system. Therefore, both test results can validate that the proposed speed control system has better parameter robustness. An acceptable range of χ in the ADRC speed control system can achieve $\chi \in (0.1, 3)$, while $\chi \in (0.1, 10)$ can be applied in the proposed speed control system. In addition, the proposed speed control system can get the consistent speed dynamic response, and tuning α can easily improve the speed loop parameter uncertainty effect on the speed control performance.

2) Rated Speed Condition: The rated speed performance of the proposed digital speed control system is validated from standstill to rated speed condition. $\omega_c, \omega_{\text{spd}}$, and ω_{ob} are set to $2\pi 300$, $2\pi 100$, and $2\pi 50\text{rad/s}$, respectively. The load torque is set from 0 to 1 N $\cdot$ m at -5.2 s. Fig. 17 shows the measured speed, measured dq-axis currents, measured one-phase current, and estimated external load torque disturbances from the proposed speed observer. It can be seen that the speed is able to track the reference speed without overshoot from the standstill to rated speed condition. Furthermore, when the external load torque is suddenly added in the system, the control system is able to reject the external disturbance, which can effectively validate the correctness of the proposed digital speed control system.

3) Current Loop Decoupling Ability: Employing the fourth-order speed observer in this section, the comparison of current loop decoupling ability speed performance of three methods can be shown in Fig. 18. In this test, ω_{spd} of the ADRC, PI-type, and proposed speed controllers is, respectively, set to $2\pi 40\text{rad/s}$, about 0.5 times $2\pi 40\text{rad/s}$, and 1.554 times $2\pi 40\text{rad/s}$ to keep the approximately same value of the cutoff frequency of the speed closed-loop system. ω_c and ω_{ob} are, respectively, set to $2\pi 100$ and $2\pi 50\text{rad/s}$, and the speed rises from 1000 r/min to rated speed. It can be seen that the minimum speed overshoot

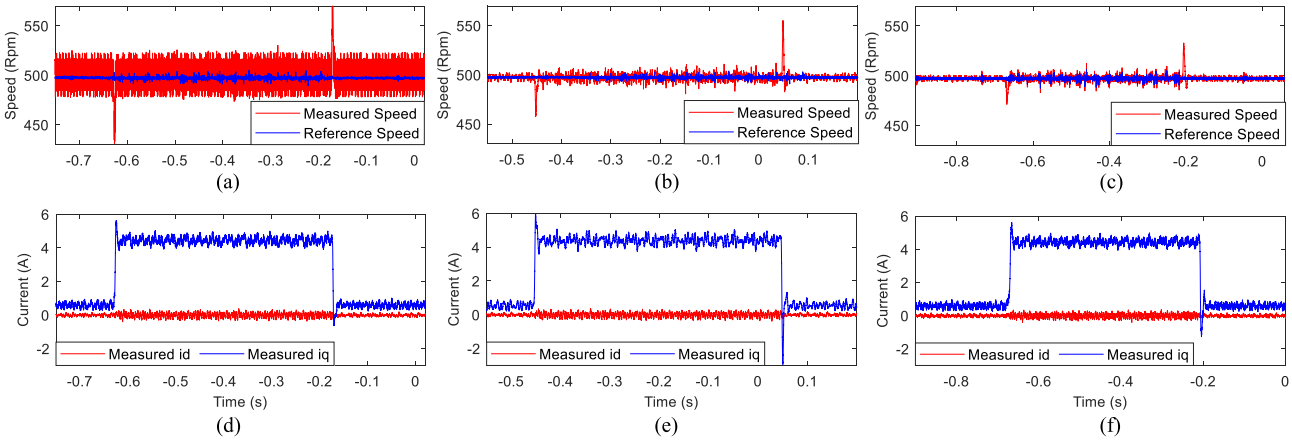

Fig. 12. Speed disturbance rejection comparison of three speed controllers. (a) and (d) ADRC speed controller. (b) and (e). PI-type speed controller. (c) and (f) Proposed speed controller.

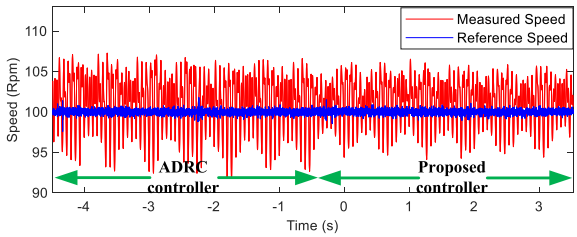

Fig. 13. Measurement noise suppression comparison of ADRC and proposed speed controllers under 100 r/min speed condition.

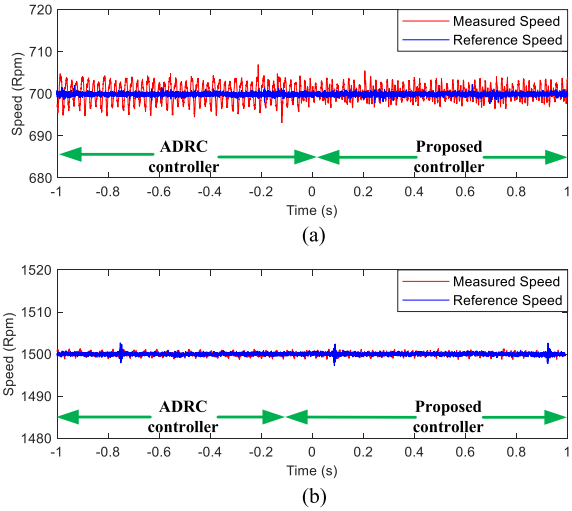

Fig. 14. Measurement noise suppression comparison of ADRC and proposed speed controllers under 700 and 1500 r/min speed conditions.

and shortest speed setting time is the proposed speed controller. Therefore, it can be validated that the current loop bandwidth can deteriorate the PI and ADRC speed controller performance, while the proposed speed controller can decouple the current loop effect on the overall speed control system.

4) Speed Controller Computation Time: Based on the system clock (200 MHz) of the TMS320F28377 digital signal processor, the calculation burden can be easily evaluated. The computation

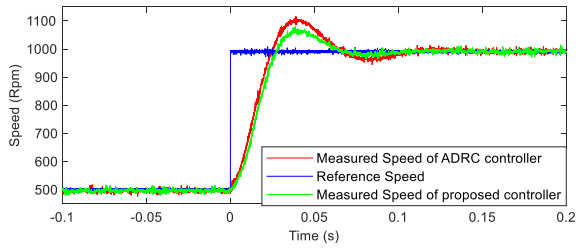

Fig. 15. Speed dynamic response comparison of ADRC and proposed speed controllers under parameter mismatch $\frac{\bar{J}}{K_t} = \frac{J}{4K_t}$.

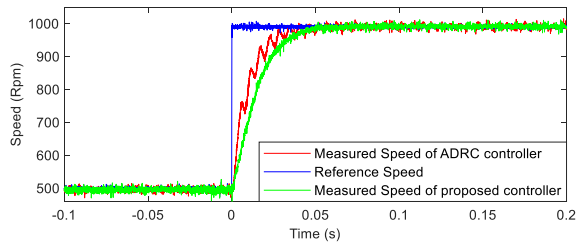

Fig. 16. Speed dynamic response comparison of ADRC and proposed speed controllers under parameter mismatch $\frac{\bar{J}}{K_t} = \frac{4J}{K_t}$.

time of the PI-type, ADRC, and proposed speed controllers is 1.3, 0.7, and 3.7 μs, respectively.

5) Overall Speed Performance Comparison: Finally, the overall performance comparison of the three speed control systems is carried out. The ADRC speed control system (System1) includes the P-type speed controller, the PI-type current controller, and the third-order speed observer, which can estimate the speed and disturbances at the same time [8], [34]. The PI-type speed control system (System2) includes the conventional PI-type speed controller, the PI-type current controller, and the third-order speed observer [8], [34]. The proposed digital speed control system (proposed system) includes the proposed speed controller with an active damping structure considering the current loop model, the PI-type current controller, and the

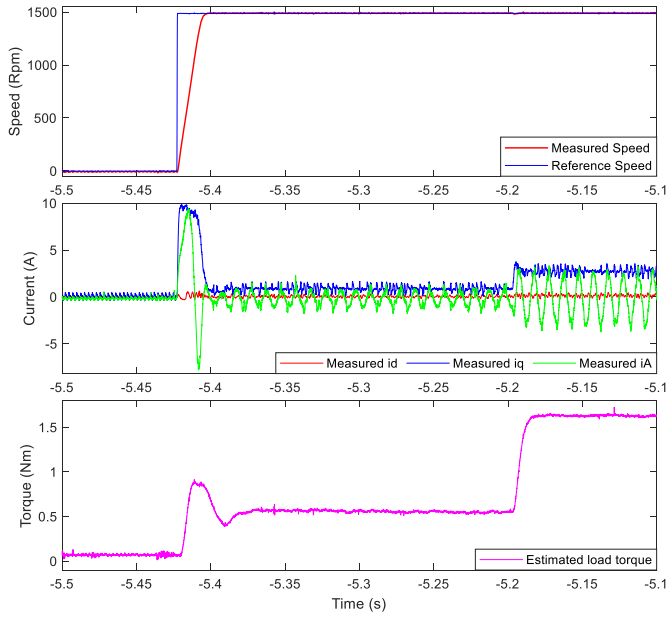

Fig. 17. Proposed digital speed control system performance under rated speed condition.

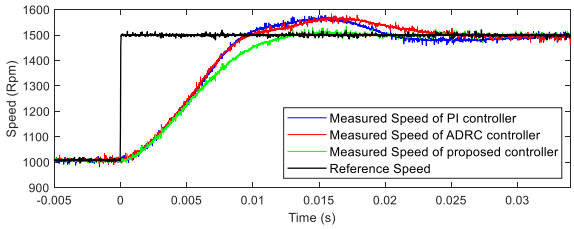

Fig. 18. Current loop decoupling ability speed performance comparison of PI, ADRC, and proposed speed controllers.

TABLE II
OVERALL PERFORMANCE OF THREE SPEED CONTROL SYSTEMS

Speed Control System Types	Dynamic Response	Disturbance Rejection	Measurement Noise Suppression	Parameter Robustness	System Complexity
System1 [8], [34]	Best	Bad	Good	Good	Lowest
System2 [8], [34]	Bad	Good	Good	Bad	Low
Proposed System	Best	Best	Best	Best	Medium

proposed fourth-order IMC speed observer. The overall performance evaluation comparison considering the current loop model is listed in Table II.

V. CONCLUSION

Based on linear control theory, a digital speed control system for PMSMs is designed theoretically. It mainly includes three parts: the proposed speed controller with active damping considering a current loop model, the proposed IMC speed observer, and the current controller.

From the experimental results, it can be seen that the correctness of the proposed speed control system analysis is able to be verified. In terms of the measurement speed part, the proposed IMC speed observer can unify other types of speed observers. The third- and fourth-order IMC speed observers have been compared to testify that higher order IMC speed observers have better quantization noise suppression, but the stability will be gradually reduced. In the proposed speed controller, the disturbance rejection, measurement noise suppression, and dynamic response is improved compared with other speed controllers. Moreover, the current loop bandwidth can be decoupled by the proposed structure. Finally, based on the designed two parts, i.e., the proposed speed controller and observer, the proposed digital speed control system has better speed loop parameter robustness though the complexity is relatively higher compared with the ADRC and PI-type speed control systems. Based on the speed dynamic response performance, the robust coefficient α can be easily tuned to improve speed loop parameter uncertainty because of the speed performance consistency between the proposed speed controller and observer.

The future perspective for this article is shown as follows. The trapezoidal reference speed tracking can be achieved by adding a simple feedforward term. The prefiltering structure can also be added to decouple the speed closed-loop sensitivity and complementary sensitivity transfer functions. Moreover, a two-DOF speed controller can be directly achieved in the proposed structure by employing a DOB or a speed observer in the speed loop feedforward path. Overall, the proposed digital speed control system can be effectively used in the servo drive systems and other high-performance industrial applications.

APPENDIX A
DESIGN OF FOURTH-ORDER SPEED OBSERVER COEFFICIENTS

$$\begin{aligned}
a_1 &= T_s^4\omega_{\text{ob}}^4 + 4T_s^3\omega_{\text{ob}}^3 + 6T_s^2\omega_{\text{ob}}^2 + 4T_s\omega_{\text{ob}} + 1\\
a_2 &= T_s^4\omega_{\text{ob}}^4 + 8T_s^3\omega_{\text{ob}}^3 + 18T_s^2\omega_{\text{ob}}^2 + 16T_s\omega_{\text{ob}} + 5\\
a_3 &= -4T_s^3\omega_{\text{ob}}^3 - 18T_s^2\omega_{\text{ob}}^2 - 24T_s\omega_{\text{ob}} - 10\\
a_4 &= 6T_s^2\omega_{\text{ob}}^2 + 16T_s\omega_{\text{ob}} + 10, \quad a_5 = -4T_s\omega_{\text{ob}} - 5\\
b_1 &= 4T_s\omega_{\text{ob}} + 1, \quad b_2 = -4(3T_s\omega_{\text{ob}} + 1)\\
b_3 &= 6(2T_s\omega_{\text{ob}} + 1), \quad b_4 = -4(T_s\omega_{\text{ob}} + 1).
\end{aligned} \tag{24}$$

APPENDIX B
DERIVATION OF THE PREDICTED LOAD-TORQUE DISTURBANCE TRANSFER FUNCTION $\frac{\hat{T}_l(s)}{T_l(s)}$ OF (6)

Without considering $\overline{J}$ and $\overline{K_t}$ parameter mismatch, substituting (3) into (4), the predicted load-torque disturbance transfer function $\frac{\hat{T}_l(s)}{T_l(s)}$ of the instantaneous speed observer [8] can be derived as

$$\begin{cases} e_\theta(s) = \theta_m(s) - \hat{\theta}_m(s) \\ e_\theta(s) = \frac{-T_l(s)+\hat{T}_l(s)-K_p e_\theta(s)-sK_d e_\theta(s)}{\overline{J}s^2}. \end{cases} \tag{25}$$

Substituting $e_\theta(s) = \frac{-s\hat{T}_l(s)}{K_i}$ of (4) into (25), (25) can be rearranged as

$$\frac{\hat{T}_l(s)(K_i + K_p s + K_d s^2) - T_l(s)K_i}{K_i\overline{J}} = \frac{-\overline{J}s^3\hat{T}_l}{K_i\overline{J}}$$

$$\frac{\hat{T}_l(s)(\overline{J}s^3 + K_i + K_p s + K_d s^2) - T_l(s)K_i}{K_i \overline{J}} = 0. \quad (26)$$

Based on $K_p = 3\omega_{\text{ob}}^2 \overline{J}$, $K_i = \omega_{\text{ob}}^3 \overline{J}$, and $K_d = 3\omega_{\text{ob}} \overline{J}$, the predicted load-torque disturbance transfer function $\frac{\hat{T}_l(s)}{T_l(s)}$ of (6) can be presented as follows:

$$\frac{\hat{T}_l(s)}{T_l(s)} = \frac{\omega_{\text{ob}}^3}{(s + \omega_{\text{ob}})^3}. \quad (27)$$

REFERENCES

[1] P. Pillay and R. Krishnan, "Application characteristics of permanent magnet synchronous and brushless DC motors for servo drives," *IEEE Trans. Ind. Appl.*, vol. 27, no. 5, pp. 986–996, Sep./Oct. 1991.

[2] X. Yuan, J. Chen, C. Jiang, and C. H. Lee, "Discrete-time current regulator for AC machine drives," *IEEE Trans. Power Electron.*, vol. 37, no. 5, pp. 5847–5858, May 2022.

[3] X. Yuan and C. H. T. Lee, "A simple three-degree-of-freedom digital current controller with dead beat response for AC machines," *IEEE Trans. Ind. Electron.*, to be published, doi: 10.1109/TIE.2021.3109540.

[4] Q. Ni *et al.*, "A new position and speed estimation scheme for position control of PMSM drives using low-resolution position sensors," *IEEE Trans. Ind. Appl.*, vol. 55, no. 4, pp. 3747–3758, Jul./Aug. 2019.

[5] T. Shi, Z. Wang, and C. Xia, "Speed measurement error suppression for PMSM control system using self-adaption Kalman observer," *IEEE Trans. Ind. Electron.*, vol. 62, no. 5, pp. 2753–2763, May 2015.

[6] T. Wang, Z.-Q. Zhu, N. M. A. Freire, Z. Wu, M. Foster, and D. A. Stone, "Study on noise and disturbance issues of generalized predictive speed control for permanent magnet synchronous machines," *IET Electr. Power Appl.*, vol. 15, pp. 63–78, 2021.

[7] C. F. Christiansen, R. Battaiotto, D. Fernandez, and E. Tacconi, "Digital measurement of angular velocity for speed control," *IEEE Trans. Ind. Electron.*, vol. 36, no. 1, pp. 79–83, Feb. 1989.

[8] R. D. Lorenz and K. W. Van Patten, "High-resolution velocity estimation for all-digital, AC servo drives," *IEEE Trans. Ind. Appl.*, vol. 27, no. 4, pp. 701–705, Jul./Aug. 1991.

[9] K. Łakomy and R. Madonski, "Cascade extended state observer for active disturbance rejection control applications under measurement noise," *ISA Trans.*, vol. 109, pp. 1–10, 2021.

[10] S.-M. Yang and S.-J. Ke, "Performance evaluation of a velocity observer for accurate velocity estimation of servo motor drives," *IEEE Trans. Ind. Appl.*, vol. 36, no. 1, pp. 98–104, Jan./Feb. 2000.

[11] D. Xu, W. Hong, and S. Jingzhuo, "PMSM servo system with speed and torque observer," in *Proc. IEEE 34th Annu. Conf. Power Electron. Spec.*, 2003, pp. 241–245.

[12] S.-H. Song and S.-K. Sul, "An instantaneous speed observer for low speed control of ac machine," in *Proc. 13th Annu. Appl. Power Electron. Conf. Expo.*, 1998, pp. 581–586.

[13] A. Yoo, S.-K. Sul, D.-C. Lee, and C.-S. Jun, "Novel speed and rotor position estimation strategy using a dual observer for low-resolution position sensors," *IEEE Trans. Power Electron.*, vol. 24, no. 12, pp. 2897–2906, Dec. 2009.

[14] M. Jemli, H. B. Azza, M. Boussak, and M. Gossa, "Sensorless indirect stator field orientation speed control for single-phase induction motor drive," *IEEE Trans. Power Electron.*, vol. 24, no. 6, pp. 1618–1627, Jun. 2009.

[15] H. A. Hussain, "Tuning and performance evaluation of 2DOF PI current controllers for PMSM drives," *IEEE Trans. Transp. Electrific.*, vol. 7, no. 3, pp. 1401–1414, Sep. 2021.

[16] L. Harnefors, K. Pietilainen, and L. Gertmar, "Torque-maximizing field-weakening control: Design, analysis, and parameter selection," *IEEE Trans. Ind. Electron.*, vol. 48, no. 1, pp. 161–168, Feb. 2001.

[17] L. Harnefors, S. E. Saarakkala, and M. Hinkkanen, "Speed control of electrical drives using classical control methods," *IEEE Trans. Ind. Appl.*, vol. 49, no. 2, pp. 889–898, Mar./Apr. 2013.

[18] I. Mishra, R. N. Tripathi, and T. Hanamoto, "Two-degree-of-freedom (2DOF) speed control based FS-MPC for PMSM drives," in *Proc. 23rd Int. Conf. Elect. Mach. Syst.*, 2020, pp. 1230–1234.

[19] C. Xia, B. Ji, T. Shi, and Y. Yan, "Two-degree-of-freedom proportional integral speed control of electrical drives with Kalman-filter-based speed estimation," *IET Electr. Power Appl.*, vol. 10, no. 1, pp. 18–24, 2016.

[20] B. Wang, C. Luo, Y. Yu, G. Wang, and D. Xu, "Antidisturbance speed control for induction machine drives using high-order fast terminal sliding-mode load torque observer," *IEEE Trans. Power Electron.*, vol. 33, no. 9, pp. 7927–7937, Sep. 2018.

[21] F. Mendoza-Mondragón, V. M. Hernández-Guzmán, and J. Rodríguez-Reséndiz, "Robust speed control of permanent magnet synchronous motors using two-degrees-of-freedom control," *IEEE Trans. Ind. Electron.*, vol. 65, no. 8, pp. 6099–6108, Aug. 2018.

[22] H.-B. Shin, "New antiwindup PI controller for variable-speed motor drives," *IEEE Trans. Ind. Electron.*, vol. 45, no. 3, pp. 445–450, Jun. 1998.

[23] E. Sariyildiz, R. Oboe, and K. Ohnishi, "Disturbance observer-based robust control and its applications: 35th anniversary overview," *IEEE Trans. Ind. Electron.*, vol. 67, no. 3, pp. 2042–2053, Mar. 2020.

[24] X. Yuan, Y. Zuo, Y. Fan, and C. H. Lee, "Model-free predictive current control of SPMSM drives using extended state observer," *IEEE Trans. Ind. Electron.*, vol. 68, no. 2, pp. 993–1003, Feb. 2021.

[25] X. Yuan, C. Zhang, and S. Zhang, "Torque ripple suppression for open-end winding permanent-magnet synchronous machine drives with predictive current control," *IEEE Trans. Ind. Electron.*, vol. 67, no. 3, pp. 1771–1781, Mar. 2020.

[26] B. Ahi and M. Haeri, "Linear active disturbance rejection control from the practical aspects," *IEEE/ASME Trans. Mechatronics*, vol. 23, no. 6, pp. 2909–2919, Dec. 2018.

[27] Y.-D. Yoon, E. Jung, A. Yoo, and S.-K. Sul, "Dual observers for the disturbance rejection of a motion control system," in *Proc. IEEE Ind. Appl. Annu. Meeting*, 2007, pp. 256–261.

[28] S.-C. Yang and R. D. Lorenz, "Surface permanent-magnet machine self-sensing at zero and low speeds using improved observer for position, velocity, and disturbance torque estimation," *IEEE Trans. Ind. Appl.*, vol. 48, no. 1, pp. 151–160, Jan./Feb. 2012.

[29] G. Pellegrino, R. I. Bojoi, P. Guglielmi, and F. Cupertino, "Accurate inverter error compensation and related self-commissioning scheme in sensorless induction motor drives," *IEEE Trans. Ind. Appl.*, vol. 46, no. 5, pp. 1970–1978, Sep./Oct. 2010.

[30] B.-H. Bae and S.-K. Sul, "A compensation method for time delay of full-digital synchronous frame current regulator of PWM AC drives," *IEEE Trans. Ind. Appl.*, vol. 39, no. 3, pp. 802–810, May/Jun. 2003.

[31] L. Harnefors and H.-P. Nee, "Model-based current control of AC machines using the internal model control method," *IEEE Trans. Ind. Appl.*, vol. 34, no. 1, pp. 133–141, Jan./Feb. 1998.

[32] T. Hagglund and K. J. Astrom, *PID Controllers: Theory, Design, and Tuning*. Research Triangle, NC, USA: Int. Soc. Autom., 1995.

[33] F. Briz, M. W. Degner, and R. D. Lorenz, "Analysis and design of current regulators using complex vectors," *IEEE Trans. Ind. Appl.*, vol. 36, no. 3, pp. 817–825, May/Jun. 2000.

[34] *InstaSPIN-FOC and InstaSPIN-Motion User's Guide (Literature Number: SPRUHJ1A)*, Texas Instruments, Dallas, TX, USA, 2013.

Xin Yuan (Member, IEEE) was born in Heilongjiang, China, in 1990. He received the B.S. degree from Beijing Union University, Beijing, China, in 2013, and the M.S. degree from the North China University of Technology, Beijing, China, in 2016, and the Ph.D. degree in electrical engineering from the Beijing Institute of Technology, Beijing, China, in 2020.

He is currently a Research Fellow with the School of Electrical and Electronic Engineering, Nanyang Technological University, Singapore. He was a Research Associate with Power Electronics, Machines and Control Group, University of Nottingham, Nottingham, U.K., from January 2019 to January 2020. His research interests include ac motor drives, power converters, multiphase motor drives, and fault-tolerant strategy of motors.

Jiahao Chen (Member, IEEE) received the B.Sc. and Ph.D. degrees in electrical engineering from Zhejiang University, Hangzhou, China, in 2014 and 2019, respectively.

From September 2018 to September 2019, he was a Visiting Scholar with the University of Wisconsin–Madison, Madison, WI, USA, where he was involved in research on bearingless motors. He is currently a Postdoctoral Research Fellow with Nanyang Technological University, Singapore. His research interests include electric machines, drives, and direct-drive technologies.

Wei Liu (Member, IEEE) received the B.Eng. and M.Eng. degrees in electrical engineering from the China University of Petroleum, Beijing, China, in 2014 and 2017, respectively, and the Ph.D. degree in electrical and electronic engineering from the University of Hong Kong (HKU), Hong Kong, in 2021.

He is currently a Postdoctoral Fellow with the Department of Electrical and Electronic Engineering, HKU. He was a Visiting Researcher with Nanyang Technological University, Singapore, in 2019. His research interests include power electronics, wireless power transfer techniques, and electric vehicle technologies.

Dr. Liu was the recipient of the Power Engineering Prize from HKU and Excellent Paper Awards from international conferences in the area of electric vehicles. He is the Guest Editor for *Energies*.

Christopher H. T. Lee (Senior Member, IEEE) received the B.Eng. (First Class Hons.) and Ph.D. degrees in electrical engineering from the Department of Electrical and Electronic Engineering, The University of Hong Kong, Hong Kong, in 2009 and 2016, respectively.

He is currently an Assistant Professor with Nanyang Technological University, Singapore, and an Honorary Assistant Professor with the University of Hong Kong, Hong Kong. He was a Postdoctoral Fellow and then a Visiting Assistant Professor with the Massachusetts Institute of Technology, Cambridge, MA, USA. He has authored or coauthored one book, three book chapters, and more than 120 referred papers in his research interests. His research interests include electric machines and drives, renewable energies, and electromechanical propulsion technologies.

Dr. Lee is the recipient of many awards, including the MDPI Energies Young Investigator Award, the NRF Fellowship, the Nanyang Assistant Professorship, the Li Ka Shing Prize (the best Ph.D. thesis prize), and the Croucher Foundation Fellowship. He is an Associate Editor for the IEEE TRANSACTIONS ON INDUSTRIAL ELECTRONICS, IEEE TRANSACTIONS ON ENERGY CONVERSION, IEEE ACCESS, and *IET Renewable Power Generation*. He is a Chartered Engineer in Hong Kong.